Konrad-Zuse-Zentrum für Informationstechnik Berlin

Ronald H.W. Hoppe[1,2]   Ralf Kornhuber[2]

Multi-Grid Solution of Two Coupled Stefan Equations Arising in Induction Heating of Large Steel Slabs

[1]Technische Universität Berlin,
 FB Mathematik
 Strasse des 17. Juni 135
 D-1000 Berlin 12

[2]Konrad-Zuse-Zentrum für Informationstechnik
 Heilbronner Strasse 10
 D-1000 Berlin 31

Ronald H.W. Hoppe   Ralf Kornhuber

Multi-Grid Solution of Two Coupled Stefan Equations Arising in Induction Heating of Large Steel Slabs

Abstract

Induction heating of large steel slabs can be described by a coupled system of nonlinear evolution equations of Stefan type representing the temporal and spatial distribution of the induced magnetic field and the generated temperature within the slab. Discretizing these equations implicitly in time and by finite differences in space, at each time step the solution of a system of difference inclusions is required. For the solution of that system two multi-grid algorithms are given which combined with a nested iteration type continuation strategy to proceed in time result in computationally highly efficient schemes for the numerical simulation of the induction heating process.

Keywords: induction heating, system of two coupled Stefan equations, multi-grid algorithms.

Subject Classification: AMS(MOS): 35K60, 35R35, 65H10, 65N05, 65N20, 78A25, 78A55.

Inhalt

1. Introduction

In steel industry, for reasons of energy savings, induction heating of steel slabs is preferred to heating with fuel-fired furnaces, because approximately 87 percent of the thermal energy is generated within the slab. The principle of induction heating is as follows: an aluminum or copper conductor, being wrapped around the steel slab along its longer side, generates an alternating magnetic field thus causing eddy currents in the slab which in turn heat the slab by Joule dissipation. Due to the skin-effect the eddy currents are concentrated below the surface which results in a non-uniform distribution of the temperature. Mathematically the temporal and spatial distribution both of the induced magnetic field and of the generated temperature within the slab can be described by a coupled system of two nonlinear evolution equations, an electromagnetic equation and a heat equation. Since carbon steel undergoes a phase transition at the Curie temperature of 760° C with a jump-like behavior of the enthalpy (Figure 1), the heat equation is of Stefan type. Likewise, the magnetization characteristics can be modelled as a discontinuous curve with a jump discontinuity at zero as long as the saturation flux density is positive which happens to be the case below the Curie temperature (Figure 4). Hence, also the electromagnetic equation is of Stefan type in regions where the temperature is below the Curie point. Altogether, we thus are faced with a coupled system of two Stefan type equations.

As far as the analysis and numerical solution of the coupled system is concerned, the most advanced work so far has been done by Bossavit [2], [3]. Note, however, that for the solution of the nonlinear electromagnetic equation in one space dimension, assuming a known temperature distribution, there are earlier approaches by Gillott and Calvert [8], who use an explicit finite difference discretization (with severe stability restrictions), by Lim and Hammond [14] whose scheme is based on a modified DuFort-Frankel finite difference method and by Schulze and Andree [16] using integral equation techniques. Since the right-hand side of the heat equation, where essentially the gradient of the magnetic field enters, is rapidly oscillating, in the approach taken by Bossavit [2], [3] different time-scales for the two equations are introduced. Then, a limit analysis yields a model system with an averaged heat equation and a time-periodic electromagnetic equation the coupling being unilateral in the sense that the heat equation has the lead, and the electromagnetic equation is subordinated to it. Numerically the leading heat equation can be solved by a nonlinear Crank-Nicolsen type scheme requiring at each time step the evaluation of the averaged right-hand side. This can be done by performing a corresponding nonlinear Crank-Nicolsen scheme for the electromagnetic equation over a sufficient number of half-periods in order to

2

get a suitable approximation to the periodic solution of that equation. The resulting systems of nonlinear difference equations are solved by a nonlinear SOR technique with a local choice of the relaxation parameter ω. In particular, $\omega = 1$ is chosen for grid points where a change of phase occours while overrelaxation is performed elsewhere. Note that a corresponding SOR technique has been proposed by Elliott [7] for the numerical solution of two-phase Stefan problems. It is well known that the convergence rate of such iteration schemes deteriorates considerably with decreasing step sizes. Hence, it would be preferable to use iterative methods with a reasonable convergence rate being independent of the chosen step sizes. Such methods can be provided by the application of multi-grid techniques. Multi-grid algorithms have been originally designed for the efficient solution of elliptic boundary value problems but have also proven their usefulness in a wide variety of other type of problems [10]. Concerning two-phase Stefan problems, the authors [12] have developed two multi-grid algorithms and have shown their superiority compared to Elliott's single grid SOR technique by application to a model Stefan type equation. Actually, both algorithms solve a difference equation resulting from a discretization of the Stefan problem implicit in time and by standard finite differences in space. The first of the algorithms is based on an interpolation of the enthalpy function between its two phases in regions where a change of phase occurs and uses bilinear interpolation as prolongations and full weighted restrictions while the coarse grid correction is damped by a strictly chosen damping factor. The main features of the second multi-grid algorithm which can be derived by a duality argument from convex analysis are the use of nonlinear Gauss-Seidel iteration as a smoother and a different choice of prolongations and restrictions in regions close to the free boundary and off the free boundary. Finally, in both algorithms at each time step an approximation on the finest grid is obtained by a suitable nested iteration type continuation strategy.

In this paper, we will show how these multi-grid schemes can be effectively applied to the coupled systems of Stefan type equations describing induction heating of large steel slabs. The paper is organized as follows: in chapter 2, following Bossavit's approach, we will introduce and discuss the averaging based model system. Then, in chapter 3 the multi-grid algorithms will be presented in detail and finally, in chapter 4 numerical results will be given documenting the whole spectrum of physical phenomena arising during the induction heating process.

3

2. The Coupled Stefan Equations

We consider a steel slab of width $2a$, length $2b$ and height c $(2b > c \gg 2a)$ occupying the domain $[0, 2a] \times [0, 2b] \times [0, c]$ in Euclidian 3-space (typical dimensions are $a = 0.05m, b = 2.5m, c = 1m$). Denoting by $B = (B_1, B_2, B_3)$, $E = (E_1, E_2, E_3)$, $H = (H_1, H_2, H_3)$ and $J = (J_1, J_2, J_3)$ the vector fields representing the magnetic induction, the electric field, the magnetic field and the eddy currents density, respectively, by Faraday's law we have

$$\frac{\partial B}{\partial t} + \mathrm{rot}\, E = 0 \ . \tag{2.1}$$

According to Ohm's law, the electric field E is related to the eddy currents density J by

$$E = \varrho_\Theta J \tag{2.2}$$

while by Ampère's theorem we have

$$J = \mathrm{rot}\, H \tag{2.3}$$

where in (2.2) the scalar function ϱ_Θ stands for the electric resistivity depending on the temperature distribution $\Theta = \Theta(x, y, z, t)$ within the slab (Figure 2). Finally, the magnetic field H is related to the induction B by

$$H = \eta_\Theta(|B|)\mathrm{sgn}(B) \tag{2.4}$$

with a temperature dependent monotone function η_Θ satisfying $\eta_\Theta(0) = 0$. In the subsequent analysis, for the inverse $\beta_\Theta = \eta_\Theta^{-1}$, called the magnetization characteristics, we will assume the simplified Fröhlich's model
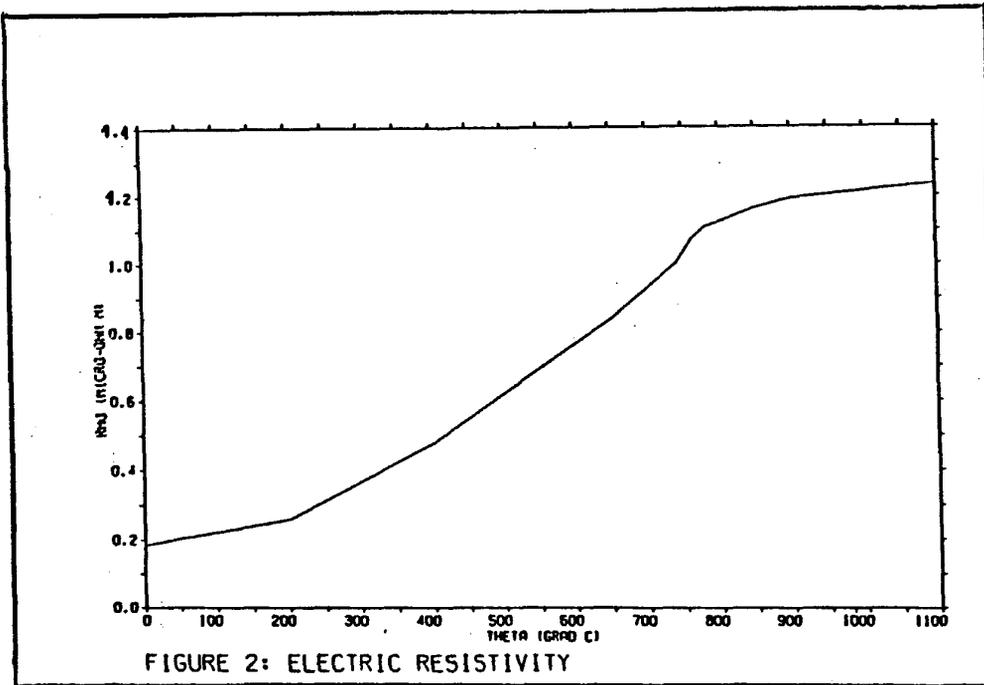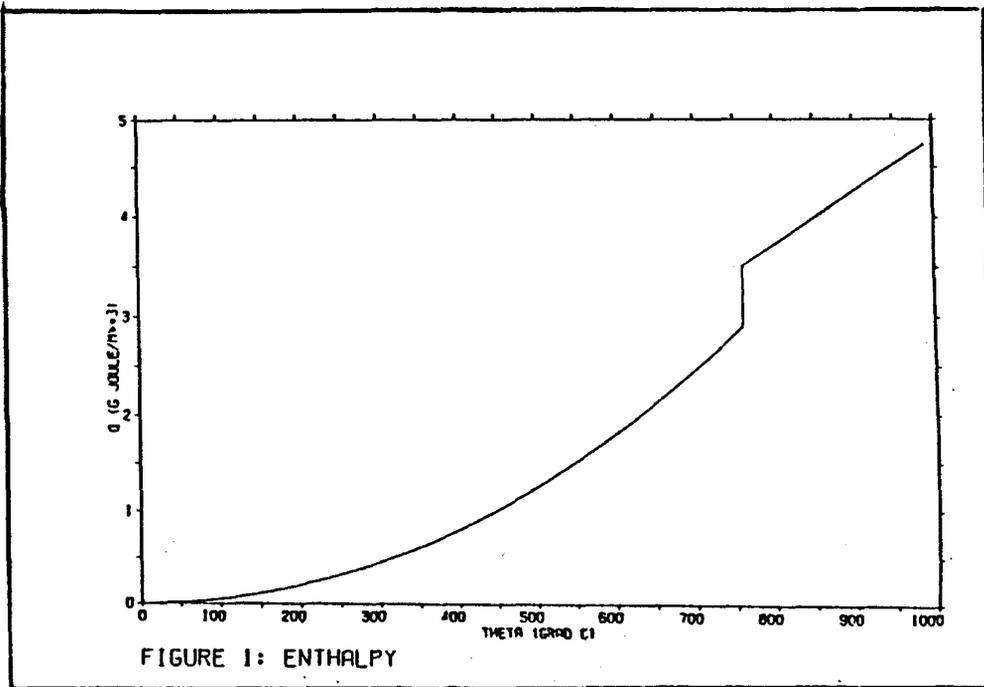
$$\beta_\Theta(s) = \mu_0 s + b_\Theta \mathrm{sgn}(s), s \in \mathbb{R} \tag{2.5}$$

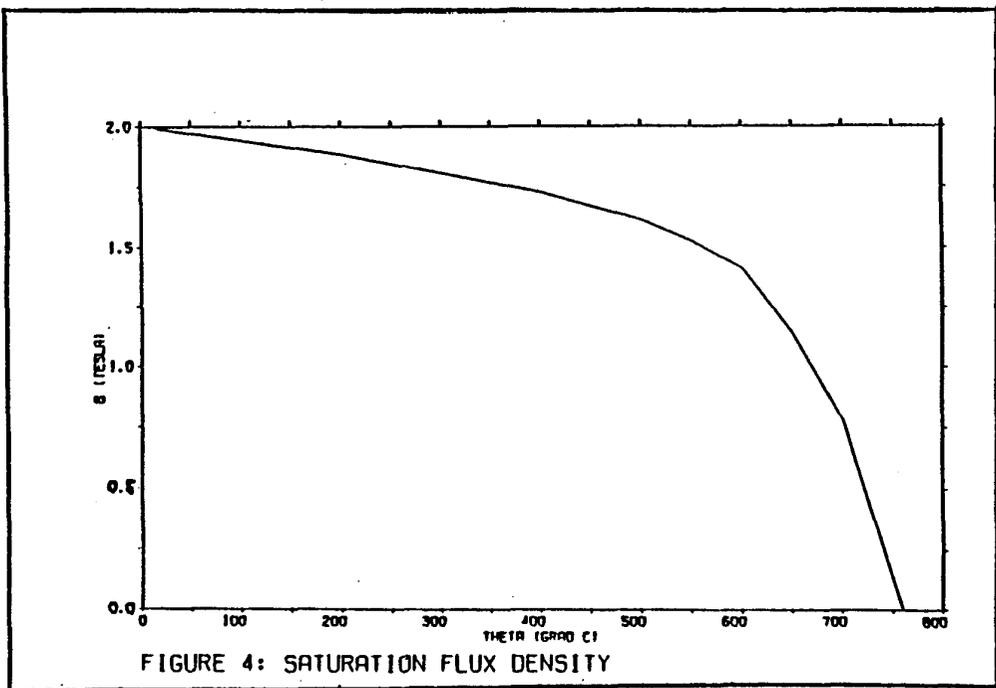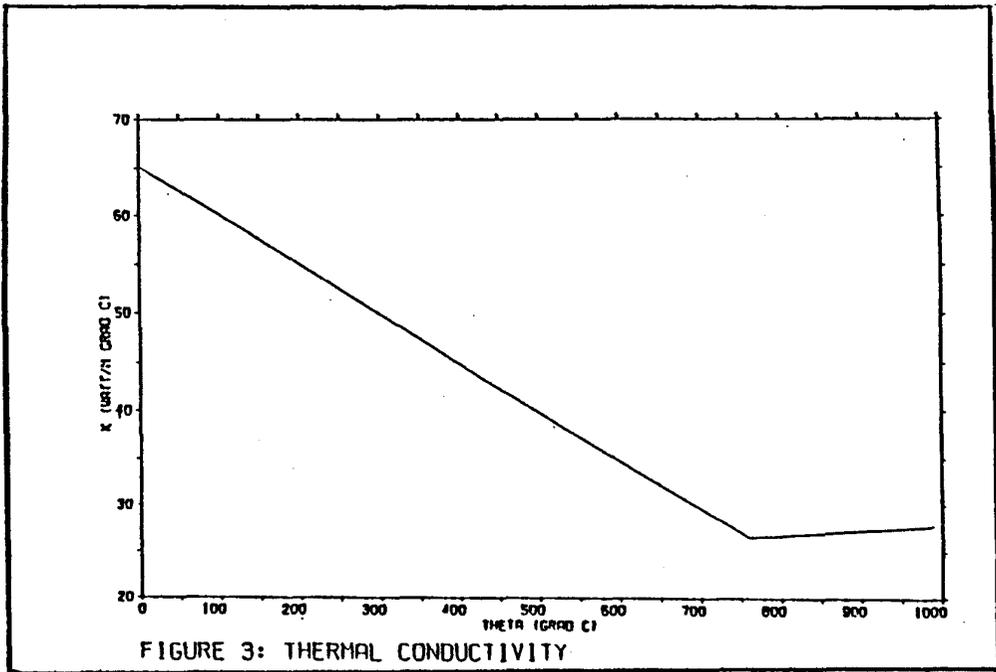with μ_0 denoting the magnetic permeability in vacuum and b_Θ the temperature dependent saturation flux density. In view of the geometric configuration of the problem – the conductor is wrapped around the longitudinal axis of the slab – the induced magnetic field H is parallel to the z-axis, i.e.,

$$H_1 \equiv 0 \ , \quad H_2 \equiv 0$$
$$H_3 = h(x, y, t) \ , \quad 0 \leq x \leq 2a \ , \quad 0 = \leq y \leq 2b \ . \tag{2.6}$$

Moreover, due to symmetry reasons we may assume

$$h(x, y, t) = h(2a - x, y, t), \ 0 \leq x \leq a$$
$$h(x, y, t) = h(x, 2b - y, t), \ 0 \leq y \leq b \ . \tag{2.7}$$

4

FIGURE 1: ENTHALPY

FIGURE 2: ELECTRIC RESISTIVITY

FIGURE 3: THERMAL CONDUCTIVITY

FIGURE 4: SATURATION FLUX DENSITY

Consequently, the problem is basically a two-dimensional one in the domain $R = (0, a) \times (0, b)$, where in view of (2.2, 2.3, 2.4, 2.5) and (2.6) the governing electromagnetic equation (2.1) reduces to

$$\frac{\partial}{\partial t} \beta_\Theta(h(x, y, t)) - \nabla \cdot (\varrho_\Theta \nabla h(x, y, t)) = 0 , \quad t > 0 . \qquad (2.8a)$$

Taking (2.7) into account, the boundary conditions are given by

$$\begin{aligned} h(x, y, t) &= \bar{h} \sin \omega t , \quad (x, y) \in \partial_1 R \\ \frac{\partial}{\partial n} h(x, y, t) &= 0 , \quad (x, y) \in \partial_2 R \end{aligned} \qquad (2.8b)$$

where $\partial_1 R = \{(x, 0) | 0 \leq x \leq a\} \cup \{(0, y) | 0 \leq y \leq b\}, \partial_2 R = \{(x, b) | 0 < x < a\} \cup \{(a, y) | 0 < y < b\}$, $\bar{h}$ denoting the amplitude and ω the frequency of the applied magnetic field. Since β_Θ has a jump discontinuity at the origin as long as $b_\Theta > 0$, the electromagnetic equation (2.8a) is of Stefan type and thus has to be interpreted in a suitable weak sense [13].

For the temperature distribution Θ within the slab we may also assume that it is constant in z-direction satisfying the same symmetry (2.7) as h. Neglecting heat exchange by radiation or convection at the slab surface, the heat equation takes the form

$$\frac{\partial}{\partial t} q(\Theta(x, y, t)) - \nabla \cdot (\kappa_\Theta \nabla \Theta(x, y, t)) = \varrho_\Theta |\nabla h(x, y, t)|^2 , \quad (x, y) \in R \quad (2.9a)$$

with zero Neumann boundary conditions

$$\kappa_\Theta \frac{\partial}{\partial n} \Theta(x, y, t) = 0 , \quad (x, y) \in \partial R \qquad (2.9b)$$

where $q = q(\Theta)$ denotes the enthalpy and κ_Θ the thermal conductivity (Figures 1,3). Since the enthalpy q exhibits a jump discontinuity at the Curie temperature of $\Theta_c = 760°C$, the heat equation (2.9a) is also of Stefan type.

In order to clarify the coupling between the electromagnetic equation (2.8a) and the heat equation (2.9a) we introduce a new time scale according to

$$\tau = \omega t \qquad (2.10)$$

and we transform the domain R onto the unit square $\Omega = (0, 1) \times (0, 1)$ by

$$x = a\xi , \quad y = b\eta . \qquad (2.11)$$

Furthermore, normalizing the electric resistivity ϱ_Θ and the saturation flux density b_Θ by

$$\varrho_\Theta = \varrho_0 r(\Theta) , \quad b_\Theta = b_0 \gamma(\Theta) \qquad (2.12)$$

7

and setting
$$h(x,y,t) = \bar{h}u(\xi,\eta,\tau) \tag{2.13}$$
the transformed boundary value problems (2.8, 2.9) are given by

$$\alpha\frac{\partial}{\partial\tau}(\gamma(\Theta)\text{sgn}(u) + \zeta^{-1}u) -$$
$$-b^2\frac{\partial}{\partial\xi}(r(\Theta)\frac{\partial u}{\partial\xi}) - a^2\frac{\partial}{\partial\eta}(r(\Theta)\frac{\partial u}{\partial\eta}) = 0 , \quad (\xi,\eta) \in \Omega \tag{2.14a}$$

$$u(\xi,\eta,\tau) = \sin\tau , \quad (\xi,\eta) \in \partial_1\Omega$$
$$\frac{\partial}{\partial n}u(\xi,\eta,\tau) = 0 , \quad (\xi,\eta) \in \partial_2\Omega \tag{2.14b}$$

where

$$\partial_1\Omega = \{(\xi,0)|0 \le \xi \le 1\} \cup \{(0,\eta)|0 \le \eta \le 1\},$$
$$\partial_2\Omega = \{(\xi,1)|0 < \xi < 1\} \cup \{(1,\eta)|0 < \eta < 1\}$$

$$a^2b^2\frac{\partial}{\partial t}q(\Theta) - b^2\frac{\partial}{\partial\xi}(\kappa_\Theta\frac{\partial\Theta}{\partial\xi} - a^2\frac{\partial}{\partial\eta}(\kappa_\Theta\frac{\partial\Theta}{\partial\eta}) =$$
$$= \varrho_0\bar{h}^2[b^2|\frac{\partial u}{\partial\xi}|^2 + a^2|\frac{\partial u}{\partial\eta}|^2] , \quad (\xi,\eta) \in \Omega \tag{2.15a}$$

$$\kappa_\Theta\frac{\partial}{\partial n}\Theta(\xi,\eta,\tau) = 0 , \quad (\xi,\eta) \in \partial\Omega . \tag{2.15b}$$

Note that in (2.14a) the constants α, ζ^{-1} are given by $\alpha = (\omega b_0 a^2 b^2)/(\varrho_0\bar{h})$ and $\zeta^{-1} = (\mu_0\bar{h})/b_0$. ($\zeta$ is commonly referred to as the Stefan number of the problem).

Since $\omega \gg 1$ in (2.10) (a typical value is $\omega = 100\pi$), we thus have a coupled system of two equations with significantly different time scales. In particular, the variation of the temperature Θ with time is slow as compared to the rate of time variation of u and the right-hand side of the heat equation (2.15a). Such systems can be conveniently handled by the method of avaraging. Following Bossavit's approach [3], we consider the time-periodic electromagnetic equation

$$\alpha\frac{\partial}{\partial\tau}(\gamma(\Theta)\text{sgn}(u) + \zeta^{-1}u) - L^I_{r(\Theta)}(u) = 0, \ (\xi,\eta) \in \Omega, \ 0 < \tau < 2\pi \tag{2.16a}$$

$$u(\xi,\eta,\tau) = \sin\tau , \quad (\xi,\eta) \in \partial_1\Omega , \ 0 \le \tau < 2\pi$$
$$\frac{\partial}{\partial n}u(\xi,\eta,\tau) = 0 , \quad (\xi,\eta) \in \partial_2\Omega , \ 0 \le \tau < 2\pi \tag{2.16b}$$

$$u(\xi,\eta,\tau) = u(\xi,\eta,\tau + 2\pi)$$

8

and the "averaged" heat equation

$$a^2 b^2 \frac{\partial}{\partial t} q(\Theta) - L_{\kappa(\Theta)}^{II}(\Theta) = f_\Theta , \quad (\xi, \eta) \in \Omega, \ t > 0 \qquad (2.17a)$$

$$\frac{\partial}{\partial n} \Theta(\xi, \eta, t) = 0 , \quad (\xi, \eta) \in \partial\Omega , \quad t > 0 \qquad (2.17b)$$

where the differential operators L^I, L^{II} and the source term f_Θ in (2.17a) are given by

$$L_{r(\Theta)}^{I}(u) = b^2 \frac{\partial}{\partial \xi}\left(r(\Theta)\frac{\partial u}{\partial \xi}\right) + a^2 \frac{\partial}{\partial \eta}\left(r(\Theta)\frac{\partial u}{\partial \eta}\right) \qquad (2.18a)$$

$$L_{\kappa(\Theta)}^{II}(\Theta) = b^2 \frac{\partial}{\partial \xi}\left(\kappa(\Theta)\frac{\partial \Theta}{\partial \xi}\right) + a^2 \frac{\partial}{\partial \eta}\left(\kappa(\Theta)\frac{\partial \Theta}{\partial \eta}\right) \qquad (2.18b)$$

$$f_\Theta = \varrho_0 \bar{h}^2 [f_\Theta^1 + f_\Theta^2] ,$$

$$f_\Theta^1 = b^2 r(\Theta)\frac{1}{2\pi} \int_0^{2\pi} \left|\frac{\partial u}{\partial \xi}(\dot{\xi}, \eta, s)\right|^2 ds , \qquad (2.19a)$$

$$f_\Theta^2 = a^2 r(\Theta)\frac{1}{2\pi} \int_0^{2\pi} \left|\frac{\partial u}{\partial \eta}(\xi, \eta, s)\right|^2 ds . \qquad (2.19b)$$

9

3. The Multi-Grid Algorithms

In this section we will discuss the application of two multi-grid algorithms in the numerical solution of the coupled system (2.16), (2.17) which have recently been developed by the authors for the solution of the classical two-phase Stefan problem [12]. Both algorithms are based on a discretization of (2.16), (2.17) implicit in time with step sizes $\Delta\tau, \Delta t$ and by standard finite differences in space with respect to a hierarchy $(\Omega_k)_{k=0}^l$ of equidistant grid point sets. As we shall see below, the discretized problems can be interpreted as difference inclusions being equivalent to variational inequalities of the second kind and unconstrained minimization problems for convex subdifferentiable functionals, respectively.

We denote by G_Θ and Q the functions given by

$$G_\Theta(s) = \alpha[\gamma(\Theta)\mathrm{sgn}(s) + \zeta^{-1}s] , \quad s \in \mathbb{R} \qquad (3.1a)$$

$$Q(s) = a^2 b^2 q(s) , \quad s \in \mathbb{R}^+ \qquad (3.1b)$$

where the graph of the enthalpy function q is shown in Figure 1. Due to the jump discontinuity of the enthalpy at the Curie temperature, Q must be interpreted as multivalued function. Moreover, in view of $\mathrm{sgn}(s) = [-1, +1]$ for $s = 0$, the same applies to G_Θ for temperatures below the Curie point.

Now, we choose step sizes $\Delta\tau = 2\pi/M$, $M \in \mathbb{N}$, and $\Delta t > 0$, and we denote by Θ^n , $u^{n,m}$ approximations to Θ , u at times $t_n = n\Delta t$, $n \in \mathbb{N}$, and $\tau_m = m\Delta\tau$, $0 \le m \le M$, respectively. Since the variations of $\kappa(\Theta)$ and $r(\Theta)$ are small during a full time period of the electromagnetic equation, we may choose $\kappa(\Theta) = \kappa(\Theta^n)$ and $r(\Theta) = r(\Theta^n)$ in (2.17a). Moreover, we discretize $f_{\Theta^n}^1$, $f_{\Theta^n}^2$ by approximating the integrals in (2.19) by the summarized trapezoidial rule for periodic functions, i.e.

$$f_{\Theta^n}^{n,1} = b^2 r(\Theta^n)\frac{\Delta\tau}{2\pi}(\frac{1}{2}|\frac{\partial u^{n,0}}{\partial\xi}|^2 + \sum_{m=1}^{M-1} |\frac{\partial u^{n,m}}{\partial\xi}|^2 + \frac{1}{2}|\frac{\partial u^{n,M}}{\partial\xi}|^2) , \qquad (3.2a)$$

$$f_{\Theta^n}^{n,2} = a^2 r(\Theta^n)\frac{\Delta\tau}{2\pi}(\frac{1}{2}|\frac{\partial u^{n,0}}{\partial\eta}|^2 + \sum_{m-1}^{M-1} |\frac{\partial u^{n,m}}{\partial\eta}|^2 + \frac{1}{2}|\frac{\partial u^{n,M}}{\partial\eta}|^2) . \qquad (3.2b)$$

Then, if we select some appropriate $G_{\Theta^n}^m \in G_{\Theta^n}(u^{n,m}), 0 \le m \le M - 1$, where $u^{n,0} = u^{n-1,M}$ for $n \ge 1$, and $Q^n \in Q(\Theta^n), n \ge 0$, the implicit time discretization of (2.16a), (2.17a) results in the differential inclusions

$$G_{\Theta^n}^m + \Delta\tau L_{r(\Theta^n)}^I(u^{n,m+1}) \in G_{\Theta^n}(u^{n,m+1}) \qquad (3.3)$$

10

$$Q^n + \Delta t L^{II}_{\kappa(\Theta^n)}(\Theta^{n+1}) + \Delta t f^n_{\Theta^n} \in Q(\Theta^{n+1}) \tag{3.4}$$

where $f^n_{\Theta^n} = \rho_0 \bar{h}^2(f^{n,1}_{\Theta^n} + f^{n,2}_{\Theta^n})$.

Remark. In view of the results by J. Jerome for the classical two-phase Stefan problem [13], for sufficiently small $\Delta\tau, \Delta t$ the differential inclusions (3.3), (3.4) with corresponding boundary conditions (2.16b), (2.17b) admit unique solutions. Moreover, for $\Delta\tau \to 0$ and $\Delta t \to 0$ the piecewise linear prolongations in time of these solutions converge in the L^2–sense to weak solutions of (2.16) (with $\gamma(\Theta) = \gamma(\Theta^n), r(\Theta) = r(\Theta^n)$) and (2.17) (with $\kappa(\Theta) = \kappa(\Theta^n), r(\Theta) = r(\Theta^n)$).

We now consider finite difference discretizations of the differential inclusions (3.3),(3.4) with respect to a hierarchy $(\Omega_k)^l_{k=0}$ of grid point sets $\Omega_k = \Omega \bigcap \mathbb{R}^2_k$ where

$$\mathbb{R}^2_k = \{(\xi_i, \eta_j)|\xi_i = ih_k, \ \eta_j = jh_k, \ i,j \in \mathbb{Z}\}$$

with step sizes $h_{k+1} = h_k/2$, $0 \le k \le l-1$, given $h_0 = 1/2$. For grid functions u_k on $\bar{\Omega}_k = \bar{\Omega} \bigcap \mathbb{R}^2_k$ we denote by $D^\pm_{k,\xi}$ and $D^\pm_{k,\eta}$ the standard forward and backward difference operators

$$D^\pm_{k,\xi} u_k(\xi,\eta) = h_k^{-1}\big[\pm u_k(\xi \pm h_k, \eta) \mp u_k(\xi,\eta)\big], \ (\xi,\eta) \in \Omega_k,$$

$D^\pm_{k,\eta}$ defined similarly. The normal derivative $\partial u/\partial n$ on $\partial\Omega$ is then approximated by $D_{k,n}u_k$ on $\partial\Omega_k = \partial\Omega \bigcap \mathbb{R}^2_k$ where $D_{k,n}u_k = D^+_{k,\xi}u_k$ $\big[D_{k,n}u_k = D^+_{k,\eta}u_k\big]$ in $(\xi,\eta) = (0,\eta_j)$ $\big[(\xi,\eta) = (\xi_i,0)\big]$ and $D_{k,n}u_k = -D^-_{k,\xi}u_k$ $\big[D_{k,n}u_k = -D^-_{k,\eta}u_k\big]$ in $(\xi,\eta) = (1,\eta_j)$ $\big[(\xi,\eta) = (\xi_i,1)\big]$, $1 \le i,j \le N_k - 1$, $N_k = 1/h_k$ while at the corners we use $D_{k,n}u_k = (D^+_{k,\xi}u_k + D^+_{k,\eta}u_k)/2$ in $(\xi,\eta) = (0,0)$ $\big[$ with similar definitions in $(0,1),(1,0)$ and $(1,1)\big]$. We approximate the elliptic differential operators $L^I_{r(\Theta^n)}$ and $L^{II}_{\kappa(\Theta^n)}$ by finite difference operators L^I_k and L^{II}_k where L^I_k is given by

$$
\begin{aligned}
L^I_k(u_k) &= b^2 D^+_{k,\xi}(r(\Theta^n_{k,i-1/2})D^-_{k,\xi}u_k) + b^2 D^-_{k,\xi}(r(\Theta^n_{k,i+1/2})D^+_{k,\xi}u_k) \\
&+ b^2 D^+_{k,\eta}(r(\Theta^n_{k,j-1/2})D^-_{k,\eta}u_k) + b^2 D^-_{k,\eta}(r(\Theta^n_{k,j+1/2})D^+_{k,\eta}u_k)
\end{aligned}
$$

with $r(\Theta^n_{k,i\pm1/2}) = \big[r(\Theta^n_k(\xi \pm h_k,\eta)) + r(\Theta^n_k(\xi,\eta))\big]/2$ and $r(\Theta^n_{k,j\pm1/2}) = \big[r(\Theta^n_k(\xi,\eta \pm h_k)) + r(\Theta^n_k(\xi,\eta))\big]/2$ while L^{II}_k is defined analogously with b^2 and $r(\cdot)$ replaced by a^2 and $\kappa(\cdot)$, respectively. Finally, we discretize $|\partial u/\partial\xi|^2$, $|\partial u/\partial\eta|^2$ in (3.2) by $(|D^+_{k,\xi}u_k|^2 + |D^-_{k,\xi}u_k|^2)/2$, where $(|D^+_{k,\eta}u_k|^2 + |D^-_{k,\eta}u_k|^2)/2$ is denoting the resulting grid functions by $f^{n,i}_{k,\Theta^n}$, $1 \le i \le 2$, and f^n_{k,Θ^n}. Then the fully discretized problems (2.16, 2.17) can be written as the following system of difference inclusions

$$G^m_{\Theta^n_k} + \Delta\tau L^I_k(u^{n,m+1}_k) \in G_{\Theta^n_k}(u^{n,m+1}_k) \tag{3.5a}$$

$$u_k^{n,m+1} = \sin \tau_{m+1}, \quad (\xi, \eta) \in \partial_1 \Omega_k = \partial_1 \Omega \cap \mathbb{R}_k^2$$
$$D_{k,n} u_k^{n,m+1} = 0, \quad (\xi, \eta) \in \partial_2 \Omega_k = \partial_2 \Omega \cap \mathbb{R}_k^2 \tag{3.5b}$$

$$Q^n + \Delta t L_k^{II}(\Theta_k^{n+1}) + \Delta t f_{k,\Theta^n}^n \in Q(\Theta_k^{n+1}) \tag{3.6a}$$

$$D_{k,n} \Theta_k^{n+1} = 0, \quad (\xi, \eta) \in \partial \Omega_k . \tag{3.6b}$$

Remark: If $u_k^{n,m}(x) = 0$ or $\Theta_k^n(x) = \Theta_c, x \in \Omega_k$, we choose $G_{\Theta_k^n}^m(x), 0 \leq m \leq M - 1$, respectively $Q^n(x)$ by

$$G_{\Theta_k^n}^m(x) = G_{\Theta_k^n}^{m-1}(x) + \Delta \tau L_k^I(u_k^{n,m})(x)$$
$$Q^n(x) = Q^{n-1}(x) + \Delta t L_k^{II}(\Theta_k^n)(x) + \Delta t f_{k,\Theta^{n-1}}^{n-1}$$

where $G_{\Theta_k^n}^{-1} = G_{\Theta_k^{n-1}}^{M-1}$.

Identifying grid functions on Ω_k with vectors in $\mathbb{R}^{N_k}$, $N_k = \text{card } \Omega_k$, with respect to the lexicographic ordering of grid points and incorporating the boundary inclusions, the conditions (3.5), (3.6) can be algebraically written as

$$b_k^I - A_k^I u_k^{n,m+1} \in G_{\Theta_k^n}(u_k^{n,m+1}) \tag{3.7}$$

$$b_k^{II} - A_k^{II} \Theta_k^{n+1} \in Q(\Theta_k^{n+1}) \tag{3.8}$$

where the (N_k, N_k)-matrices A_k^I, A_k^{II} denote the matrix representations of the difference operators $-\Delta \tau L_k^I, -\Delta t L_k^{II}$ and b_k^I, b_k^{II} are appropriately defined vectors in $\mathbb{R}^{N_k}$.

In the sequel we will present two multi-grid methods for the numerical solution of (3.7) and (3.8). For simplification the schemes will only be described as applied to (3.7). Furthermore, for notational convenience the superscripts I, n and $m + 1$ in (3.7) will be omitted.

The first multi-grid algorithm is based on the idea to replace the inclusion (3.7) by an equivalent nonlinear algebraic systems which is then solved using Brandt's FAS algorithm [4] combined with damping of the interpolated coarse grid correction. Setting $A_k = (a_{ij}^k)_{i,j=1}^{N_k}$ and

$$\lambda_{k,i}(u_k) = \left(b_{k,i} - \sum_{\substack{j=1 \\ j \neq i}}^{N_k} a_{ij}^k u_{k,j} + \alpha \gamma(\Theta_{k,i}) \right) / 2\alpha\gamma(\Theta_{k,i}), \quad 1 \leq i \leq N_k ,$$

it is easily seen from (3.1a) and (3.7) that the two phases $u_{k,i} < 0$, $u_{k,i} > 0$ and the change of phase $u_{k,i} = 0$ can be characterized by $\lambda_{k,i}(u_k)$ according

12

to

$$
\left.\begin{array}{l}
u_{k,i} < 0 \\
u_{k,i} = 0 \\
u_{k,i} > 0
\end{array}\right\} \iff \left\{\begin{array}{l}
\lambda_{k,i}(u_k) < 0 \\
\lambda_{k,i}(u_k) \in [0,1] \\
\lambda_{k,i}(u_k) > 1 .
\end{array}\right.
$$

Now, if $\lambda_{k,i}(u_k) \in [0,1]$ we replace the i-th component of (3.7) by

$$
b_{k,i} - (A_k u_k)_i = G^{conv}_{\Theta_{k,i}}(u_{k,i}) \tag{3.9}
$$

where $G^{conv}_{\Theta_{k,i}}(u_{k,i})$ is the following convex combination

$$
\begin{aligned}
G^{conv}_{\Theta_{k,i}}(u_{k,i}) = {} & (1 - \lambda_{k,i}(u_k)) \ \left(\alpha\zeta^{-1}u_{k,i} - \alpha\gamma(\Theta_{k,i})\right) \\
& +\lambda_{k,i}(u_k) \ \left(\alpha\zeta^{-1}u_{k,i} - \alpha\gamma(\Theta_{k,i})\right) .
\end{aligned} \tag{3.10}
$$

Obviously, (3.9) implies $u_{k,i} = 0$ and hence, defining a vector $\tilde{G}_k(u_k) \in \mathbb{R}^{N_k}$ by

$$
\tilde{G}_{k,i}(u_k) = \left\{\begin{array}{ll}
G_{\Theta_{k,i}}(u_{k,i}) , & \text{if} \quad \lambda_{k,i}(u_k) \notin [0,1] \\
G^{conv}_{\Theta_{k,i}}(u_{k,i}) , & \text{if} \quad \lambda_{k,i}(u_k) \in [0,1]
\end{array}\right. \tag{3.11}
$$

the algebraic inclusion (3.7) is equivalent to the nonlinear algebraic system

$$
F_k(u_k) := b_k - A_k u_k - \tilde{G}_k(u_k) = 0 . \tag{3.12}
$$

Starting from an iterate u_l^ν , $\nu \geq 0$, on the highest level and choosing full weighted nine-point restrictions r_k^{k-1} , $1 \leq k \leq l$, Brandt's FAS scheme [4] involves the nonlinear systems

$$
F_k(u_k) = \bar{b}_k , \quad 0 \leq k \leq l \tag{3.13}
$$

where $\bar{b}_l = 0$ and $\bar{b}_k$, $0 \leq k \leq l - 1$, is recursively defined by

$$
\bar{b}_k := F_k(r_{k+1}^k \bar{u}_{k+1}^\nu) - r_{k+1}^k(F_{k+1}(\bar{u}_{k+1}^\nu) - \bar{b}_{k+1}) ,
$$

$\bar{u}_{k+1}^\nu$ denoting the result of the smoothing process on level $k + 1$. A convenient smoothing process is to perform $\kappa_k > 0$ nonlinear Gauss-Seidel iterations applied to (3.13). Choosing $u_l^{\nu,0} = u_l^\nu$ respectively $u_k^{\nu,0} = r_{k+1}^k \bar{u}_{k+1}^\nu$, $0 \leq k \leq l - 1$, as a startiterate, $\bar{u}_k^\nu$ is computed by

$$
\bar{u}_k^\nu = u_k^{\nu,\kappa_k} , \quad u_k^{\nu,\eta} = S_k(u_k^{\nu,\eta-1} ; \bar{b}_k) , \quad 1 \leq \eta \leq \kappa_k
$$

where $S_k(\cdot; \bar{b}_k)$ denotes the execution of one nonlinear Gauss-Seidel iteration step. Taking (3.10) and (3.11) into account, the components of $u_k^{\nu,\eta}$ can be easily computed by means of

$$
u_{k,i}^{\nu,\eta} = \left\{\begin{array}{l}
(d_{k,i} + \alpha\gamma(\Theta_{k,i}))/(\alpha,\zeta^{-1} + a_{ii}^k) , \text{ if } d_{k,i} < -\alpha\gamma(\Theta_{k,i}) \\
0 , \text{ if } d_{k,i} \in [-\alpha\gamma(\Theta_{k,i}) , \ +\alpha\gamma(\Theta_{k,i})] \\
(d_{k,i} - \alpha\gamma(\Theta_{k,i}))/(\alpha\zeta^{-1} + a_{ii}^k) \text{ if } d_{k,i} > +\alpha\gamma(\Theta_{k,i})
\end{array}\right. \tag{3.14}
$$

13

where

$$d_{k,i} = \bar{b}_{k,i} - \sum_{j=1}^{i-1} a_{ij}^k u_{k,j}^{\nu,\eta} - \sum_{j=i+1}^{N_k} a_{ij}^k u_{k,j}^{\nu,\eta-1}, \quad 1 \le i \le N_k.$$

Nonlinear Gauss-Seidel iteration will also be used as an iterative solver of the coarsest grid correction problem, performing at most κ_0 iterations. Finally, having computed an approximation u_{k-1} to the coarse grid problem on level $k-1$, a new iterate $u_k^{\nu+1}$ on level k is determined by

$$u_k^{\nu+1} = \bar{u}_k^{\nu} - \omega_k p_{k-1}^k (r_k^{k-1} \bar{u}_k^{\nu} - u_{k-1})$$

where p_{k-1}^k is the prolongation based on bilinear interpolation and ω_k a suitably chosen damping parameter. Note that damped nonlinear multi-grid iterations have been recently proposed by Hackbusch and Reusken [11] for the solution of discretized nonlinear elliptic boundary value problems. Alltogether, the complete multi-grid algorithm for the approximate solution of the fully discretized electromagnetic equation can be described by the following procedure MGELEC1 $(l, u_l, \bar{b}_l)$ with $u_l = u_l^{\nu}$ as input and $u_l = u_l^{\nu+1}$ as output:

```
procedure MGELEC1 (l, u_l, b_l);
integer i,l; array u_l, b_l;
if l = 0 then
      for i := 1 step 1 until κ_0 do u_0 := S_0(u_0; b_0)
else
      begin array u_{l-1}, b_{l-1};
      for i := 1 step 1 until κ_{l-1} do u_l := S_l(u_l; b_l);
      u_{l-1} := r_l^{l-1} u_l;
      b_{l-1} := F_{l-1}(r_l^{l-1} u_l) - r_l^{l-1}(F_l(u_l) - b_l);
      for i := 1 step 1 until γ_{l-1} do MGELEC1 (l - 1, u_{l-1}, b_{l-1});
      u_l := u_l - ω_l p_{l-1}^l (r_l^{l-1} u_l - u_{l-1});
      end
end MGELEC1.
```

The choice $\gamma_k = 1$ respectively $\gamma_k = 2$, $1 \le k \le l - 1$, corresponds to a V-cycle respectively W-cycle structure of the multi-grid iteration.

A suitable startiterate on the highest level can be provided by nested iteration incorporating the previously computed values u_k^m at time $t = t_m$ [10]:

```
procedure NIELEC1 (l, u_l, u_l^m, b_l);
integer l; array u_l, u_l^m, b_l;
begin integer i,k;
for k := 0 step 1 until l - 1 do
      if k = 0 then u_k = u_k^m
```

14

```
else
        u_k := u_k^m + p_{k-1}^k(u_{k-1} - u_{k-1}^m);
        for i := 1 step 1 until τ_k do MGELEC1 (k, u_k, b̄_k);
u_l := u_l^m + p̃_{l-1}^l(u_{l-1} - u_{l-1}^m);
end NIELEC1.
```

The second multi-grid algorithm can be derived by making use of some elementary facts from convex analysis. In particular, the multivalued function G_Θ as given by (3.1a) appears to be the subgradient $\partial\Phi_\Theta$ of the piecewise quadratic function

$$\Phi_\Theta(s) = \frac{1}{2}\alpha\zeta^{-1}s^2 + \alpha\gamma(\Theta)(s_+ - s_-)$$

where $s_+ = \max(s, 0)$ and $s_- = \min(s, 0)$. Setting

$$\varphi_{\Theta_k}(u_k) = \sum_{i=1}^{N_k} \Phi_{\Theta_{k,i}}(u_{k,i}) \;, \quad a_k(u_k, v_k) = \langle A_k u_k, v_k \rangle$$

where $\langle \cdot, \cdot \rangle$ denotes the Euclidean scalar product in $\mathbb{R}^{N_k}$, the inclusion (3.7) is equivalent to the nonlinear variational inequality

$$a_k(u_k, v_k - u_k) - \langle b_k, v_k - u_k \rangle + \varphi_{\Theta_k}(v_k) - \varphi_{\Theta_k}(u_k) \geq 0 \;, \quad v_k \in \mathbb{R}^{N_k} \;. \quad (3.15)$$

Due to the appearance of the subdifferentiable functional φ_{Θ_k}, such inequalities are commonly referred to as variational inequalities of the second kind [9]. Moreover, (3.15) is the necessary and sufficient optimality condition for the unconstrained minimization of the subdifferentiable convex functional

$$J_k(u_k) = \frac{1}{2}a_k(u_k, u_k) - \langle b_k, u_k \rangle + \varphi_{\Theta_k}(u_k) \;. \quad (3.16)$$

For variational inequalities of type (3.15) Elliott [7] has developed a nonlinear SOR technique with relaxation parameter $\omega = 1$ when change of phase occurs and overrelaxation elsewhere which results in a globally convergent minimizing sequence for the functional J_k. Since nonlinear SOR iteration suffers from poor convergence rates for decreasing step sizes but is known to yield good smoothing rates within a multi-grid framework, we will use a multi-grid approach to the problem at hand. The difficulty to deal with inclusions can be circumvented by taking advantage of the well known equivalence [6]

$$b_k - A_k u_k \in \partial\Phi_{\Theta_k}(u_k) \Leftrightarrow u_k \in \partial\Phi_{\Theta_k}^*(b_k - A_k u_k) \quad (3.17)$$

where $\Phi_{\Theta_k}^*$ stands for the Fenchel conjugate of Φ_{Θ_k}. Here, Φ_Θ^* can be easily computed giving

$$\Phi_\Theta^*(s) = \frac{1}{2}\alpha^{-1}\zeta(s - \alpha\gamma(\Theta))_+^2 + \frac{1}{2}\alpha^{-1}\zeta(s + \alpha\gamma(\Theta))_-^2$$

so that its subgradient $\partial\Phi_\Theta^*$ turns out to be the piecewise linear continuous function.

$$\partial\Phi_\Theta^*(s) = \begin{cases} \alpha^{-1}\zeta(s + \alpha\gamma(\Theta)) \,, & s < -\alpha\gamma(\Theta) \\ 0 \,, & s \in [-\alpha\gamma(\Theta), +\alpha\gamma(\Theta)] \\ \alpha^{-1}\zeta(s - \alpha\gamma(\Theta)) \,, & s > +\alpha\gamma(\Theta). \end{cases} \tag{3.18}$$

Consequently, the second inclusion in (3.17) reduces to the nonlinear algebraic system

$$u_k = \partial\Phi_{\Theta_k}^*(b_k - A_k u_k)$$

and it is that nonlinear system which will be solved by Brandt's FAS scheme using nonlinear Gauss-Seidel iteration a a smoother and an adaptive local choice of restrictions and prolongations in the fine-to-coarse and coarse-to-fine transfers of the multi-grid cycles. The FAS scheme gives rise to the nonlinear systems

$$F_k(u_k) = u_k - \partial\Phi_{\Theta_k}^*(\bar{b}_k - A_k u_k) = 0 \,, \quad 0 \leq k \leq l \,, \tag{3.19}$$

where $\bar{b}_l = b_l$ and

$$\bar{b}_k = A_k r_{k+1}^k \bar{u}_{k+1}^\nu - r_{k+1}^k(A_{k+1}\bar{u}_{k+1}^\nu - \bar{b}_{k+1}) \,, \quad 0 \leq k \leq l-1 \,,$$

$\bar{u}_{k+1}^\nu$ again denoting the result of the smoothing process on level $k+1$. Regarding (3.18), the components of the Gauss-Seidel iterates can be computed in the same way as described by (3.14).

As far as the restrictions r_k^{k-1} , $1 \leq k \leq l$, are concerned we remark that full weighted nine-point restriction cannot be used globally, since otherwise it is not guaranteed that the solution u_l^* to (3.19) on level l is a fixed point of the multi-grid iteration. The reason is that for coarse grid point with fine grid neighbours corresponding to different phases the full weighted restricted defect is not a reliable indicator of the accuracy of the approximation [12]. To remedy that inconvenience we decompose the grid point sets Ω_k , $0 \leq k \leq l$, according to

$$\Omega_k = \Omega_k^1((u_k) \cup \Omega_k^2(u_k) \cup \Sigma_k(u_k)$$

where

$$\Omega_k^i(u_k) = \{x \in \Omega_k | (-1)^i u_k(x) > 0\} \,, \quad i = 1, 2$$
$$\Sigma_k(u_k) = \{x \in \Omega_k | u_k(x) = 0\}$$

and we define $N_k(x), x \in \Omega_k$, as the set consisting of $x \in \Omega_k$ and its eight neighbouring grid points in Ω_k, i.e. $N_k(x) = \{x, x \pm h_k e_k^j \mid 1 \leq j \leq 4\} \cap \Omega_k$, where $e_k^1 = (1, 0)$, $e_k^2 = (0, 1)$, $e_k^3 = e_k^1 + e_k^2$, $e_k^4 = e_k^1 - e_k^2$. Then a grid point $x \in \Omega_k$ will be called regular, if $N_k(x) \subseteq \Omega_k(u_k)$, $i \in \{1, 2\}$, or $N_k(x) \subseteq \Sigma_k(u_k)$, and irregular otherwise. Denoting by $\hat{r}_k^{k-1}$ full

16

weighted nine-point restriction and by $\overset{\circ}{r}_k^{k-1}$ pointwise restriction, we choose r_k^{k-1} according to

$$(r_k^{k-1}u_k)(x) = \begin{cases} (\hat{r}_k^{k-1}u_k)(x) & , \quad \text{if } x \text{ is regular} \\ (\overset{\circ}{r}_k^{k-1}u_k)(x) & , \quad \text{if } x \text{ irregular.} \end{cases}$$

Moreover, a change of phase should not be caused by the coarse-to-fine transfer but only by the smoothing process, since otherwise an oscillatory behaviour of the iterates will occur in a vicinity of the discrete free boundary. For that reason denoting by $\hat{p}_{k-1}^k$ prolongation based on bilinear interpolation, a convenient choice of p_{k-1}^k is

$$(p_{k-1}^k u_{k-1})(x) = \begin{cases} (\hat{p}_{k-1}^k u_{k-1})(x) & , \quad \text{if } x \text{ is regular} \\ 0 & , \quad \text{if } x \text{ is irregular.} \end{cases}$$

The complete multi-grid algorithm can be described by the following procedure MGELEC2 $(l, u_l, \bar{b}_l)$:

```
procedure MGELEC2 (l,uₗ,b̄ₗ);
integer i,l; array uₗ,b̄ₗ;
if l = 0 then
      for i := 1 step 1 until κ₀ do u₀ := S₀(u₀;b̄₀);
else
      begin array uₗ₋₁,b̄ₗ₋₁;
      for i := 1 step 1 until κₗ¹ do uₗ := Sₗ(uₗ;b̄ₗ);
      uₗ₋₁ := rₗˡ⁻¹uₗ;
      b̄ₗ₋₁ := Aₗ₋₁rₗˡ⁻¹uₗ − rₗˡ⁻¹(Aₗuₗ − b̄ₗ);
      for i := 1 step 1 until γₗ₋₁ do MGELEC2 (l − 1,uₗ₋₁,b̄ₗ₋₁);
      uₗ := uₗ − pₗ₋₁ˡ(rₗˡ⁻¹uₗ − uₗ₋₁);
      for i := 1 step 1 until κₗ² do uₗ := Sₗ(uₗ;b̄ₗ);
      end
end MGELEC2.
```

Note that κ_k^1 and κ_k^2, $1 \le k \le l$, stand for the numbers of pre- and post-smoothings while κ_0 is the maximal number of nonlinear Gauss-Seidel interations for solving the coarsest grid correction problem on level $k = 0$. The use of nonlinear Gauss-Seidel iteration as an iterative solver for the coarsest grid correction problem is justified by the fact that the mappings F_k defined by means of (3.19) can be shown to be continuous surjective M-functions for which the iteration is known to be globally convergent [15]. Moreover, using elementary subdifferential calculus [5] and nonlinear multi-grid convergence theory in the spirit of Hackbusch [10], local convergence of the multi-grid algorithm MGELEC2 can be established [12].

17

Finally, a startiterate on the highest level l can be obtained by the nested iteration algorithm NIELEC2 which is literally the same as NIELEC1 except that MGELEC1 has to be replaced by MGELEC2. The second algebraic inclusion (3.8), representing the fully discretized heat equation, can be solved numerically by the same multi-grid techniques as described above. Without giving details the corresponding multi-grid algorithms will be denoted by MGHEAT1, NIHEAT1, MGHEAT2 and NIHEAT2, respectively.

The efficiency of the two multi-grid algorithms has been tested for a model two-phase Stefan problem exhibiting a step-size independent convergence rate compared to a deteriorating convergence rate with decreasing step-size for Elliott's single-grid SOR technique [12].

4. Numerical Results

The induction heating process has been numerically solved by the multi-grid algorithms MGELEC1, MGHEAT1 respectively MGELEC2, MGHEAT2 described in the preceding section for slabs of different width 2a and length 2b and for various physical data H, ω and discretization parameters, i.e., hierarchies $(\Omega_k)_{k=0}^l$ and time steps $\Delta\tau, \Delta t$. In accordance with the findings for a model two-phase Stefan problem [12], the asymptotic convergence rates of both algorithms turned out to be independent of the spatial step size compared to the typical $0(1 - h_l^2)$ behaviour of the convergence rate of Elliott's single-grid nonlinear SOR method. Moreover, for a suitable choice of the damping parameter the solution based on MGELEC1 and MGHEAT1 was faster than using MGELEC2 and MGHEAT2 by an average factor of 1.5.

In the sequel we want to document the numerical simulation of the physical phenomena arising during the induction heating process by displaying the induced magnetic field and the temperature distribution for a slab of width 0.1 m, length 2.0 m and physical data $H = 1.4 \cdot 10^6 A/m$ and $\omega = 100\pi(50Hz)$ using a hierarchy of grids with Ω_0 ($h_0 = 1/2$) as coarsest grid and Ω_4 ($h_4 = 1/32$) as finest grid as well as time step sizes $\Delta\tau = 2\pi/16$ and $\Delta t = 0.02$. Note that the amplitude $H = 1.4 \cdot 10^6 A/m$ is not physically realizable by the technical devices being available up to now, but has been chosen in the present example to speed up the induction heating process. As initial temperature we have chosen a uniform temperature distribution of $\Theta^0 = 20^0 C$. Startiterates on the finest grid have been computed by nested iteration (NIELEC1, NIHEAT1 respectively NIELEC2, NIHEAT2) followed by the execution of multi-grid V-cycles (MGELEC1, MGHEAT1 respectively MGELEC2, MGHEAT2) with one pre-smoothing and no post-smoothing until the relative error of two subsequent multi-grid iterates was less then $5 \cdot 10^{-4}$. The damping parameter both in MGELEC1 and MGHEAT1 was chosen by 0.5.

Figures 5-8 represent the induced magnetic field over the half-section $[0, a] \times [0, 2b]$ of the slab at the beginning of the heating ($t = 0.1$), after some heating ($t = 0.5$), when the surface has crossed the Curie temperature Θ_c ($t = 2.0$) and when most part of the slab has crossed Θ_c ($t = 3.0$). The plots display the magnetic field over a full period of the electromagnetic equation from $\tau_1 = 2\pi/16$ up to $\tau_{16} = 2\pi$ and have to be regarded from left to right and from top to bottom. Note that the plots do not reflect the actual geometry of the slab. For the sake of better visibility of the physical effects, the slab appears to be stretched in the x-direction. In particular, the Stefan effect, i.e., the appearance of moving boundaries, is even better visible for one-dimensional plots. Figures 9-12 show the induced magnetic field for $0 \leq x \leq a$ and fixed $y = b$ (half-length of the slab) at the same stages of the heating process as

19

in Figures 5-8. Finally, Figures 13-16 display the corresponding temperature distributions over the half-section $[0, a] \times [0, 2b]$.

At the beginning of the heating (Figures 5, 9), both the skin effect, i.e., the appearance of a dead zone which has not yet been penetrated by the electro-magnetic field, and the Stefan effect are clearly visible. In particular, at each half-period of the electromagnetic equation, a free boundary, corresponding to the change of phase of the induced magnetic field, is created at the sur-face of the slab and then wanders out to the right until it meets the dead core. Figure 13 represents the associated temperature distribution. Note that in the dead zone the temperature is only slightly above the initial room temperature.

Figures 6, 10 and 14 show the corresponding results after some duration of the heating process, but still completely in the nonlinear regime, i.e., the surface temperature is still below the Curie point by a wide margin (Figure 14). Basically, one can observe the same phenomena as in the figures discussed before with the only difference that the penetration depth has increased, i.e., the dead core has become smaller (Figures 6, 10).

A new phenomenon, namely the coexistence of a nonlinear regime below the Curie temperature Θ_c and a linear regime above Θ_c, arises when part of the slab close to the surface has crossed Θ_c (Figures 7, 11, 15). Now, the penetration depth is already larger than the half-width of the slab, i.e., the dead core effect has disappeared. The moving boundaries travel to the right up to the half-width of the slab where they meet their counterparts coming from the right-hand side of the slab and die out. Notice the almost uniform distribution of the induced magnetic field after that happens and the appearance of a certain oscillating behaviour within the boundary larger in y-direction (Plots 7, 15 in Figures 7, 11). The reason for these oscillations lies in the fact that the penetration depth is slightly larger than 0.05 m so that due to the geometry of the slab in x-direction we have a superposition of the waves coming from the left and the right while in y-direction there is still a pronounced dead core effect. As far as the associated temperature distribution is concerned (Figure 15), besides the expected temperature peaks at the corner of the slab notice the appearance of a moving boundary with respect to the heat equation: the region which appears as a step in the temperature profile corresponds to the change of phase temperature Θ_c of the heat equation where the magnetic behaviour of the steel changes from ferromagnetic to paramagnetic.

20

Finally, Figures 8, 12 and 16 display the results in the case where most part of the slab has crossed the Curie temperature Θ_c. Note that the life span of the moving boundaries for the electromagnetic equations has decreased compared to the situation before (Figures 8, 12) and that, as expected, the moving boundary for the heat equation has travelled to the right (Figure 16). All results reported in this section are based on computations which have been performed on the CRAY X-MP/24 at the Konrad-Zuse-Zentrum, Berlin.
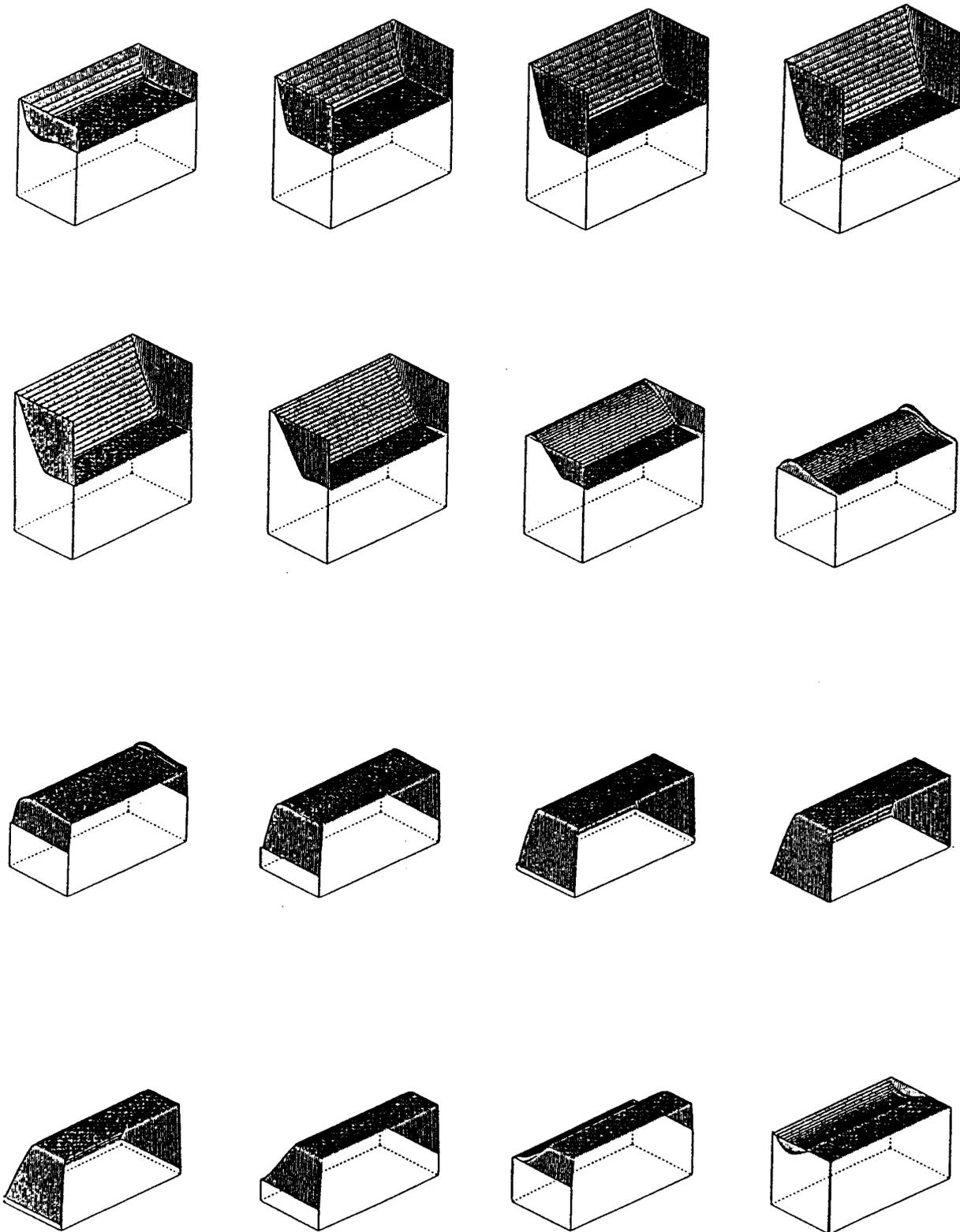
MAGNETIC FIELD
(AT THE BEGINNING OF THE HEATING)

FIGURE 5

22
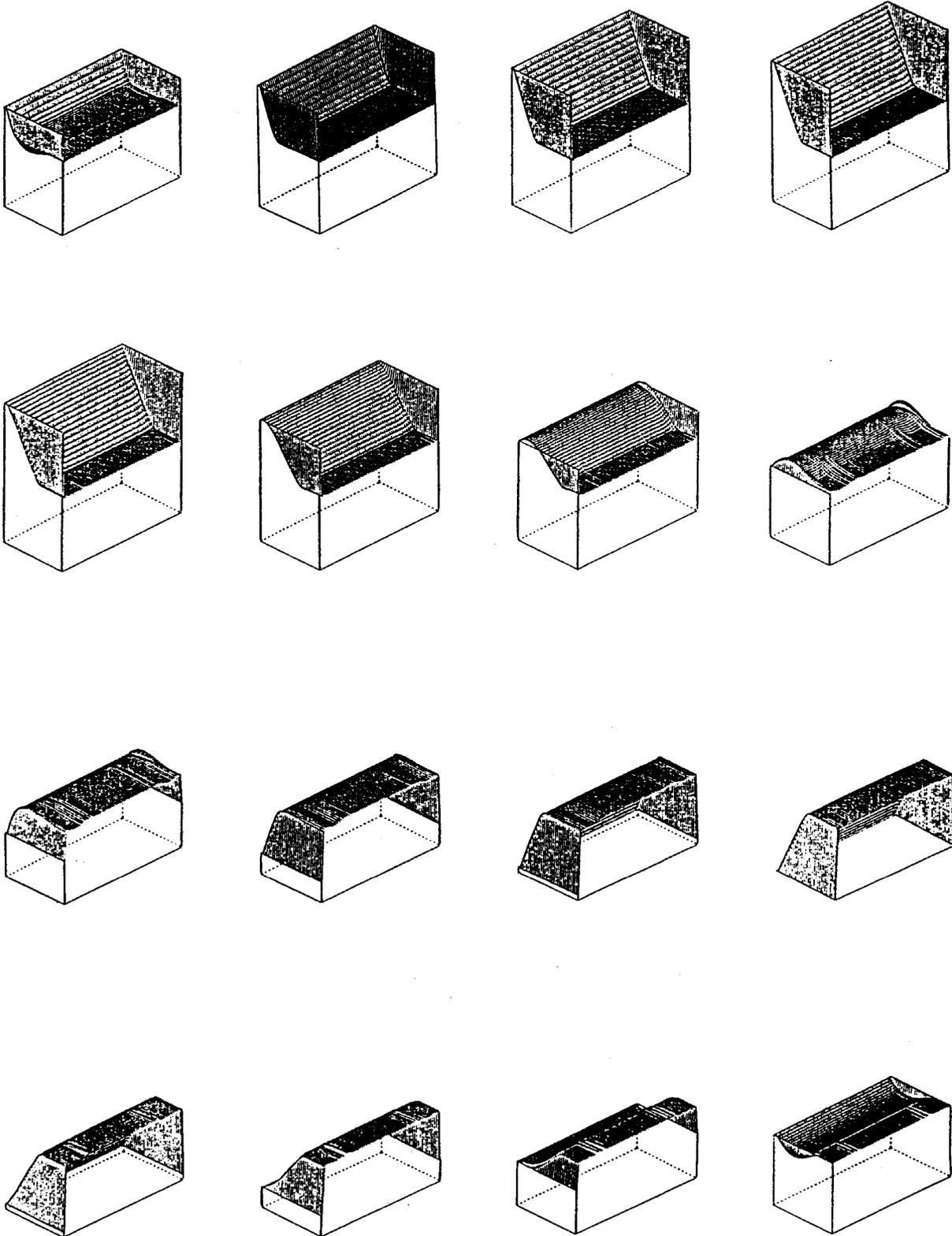
**MAGNETIC FIELD
(AFTER SOME HEATING)**

FIGURE 6
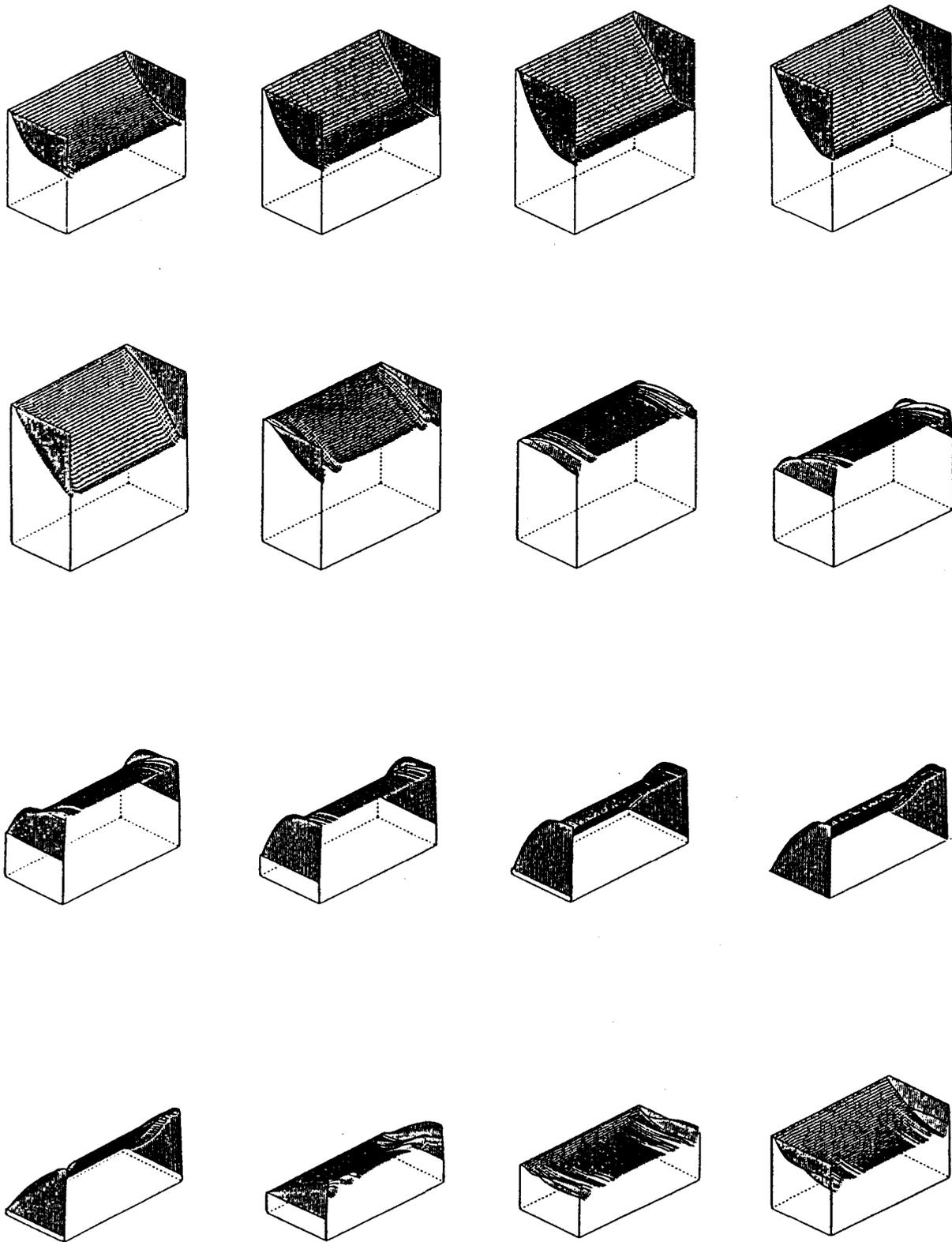
MAGNETIC FIELD
(SURFACE HAS CROSSED THE CURIE TEMPERATURE)

FIGURE 7
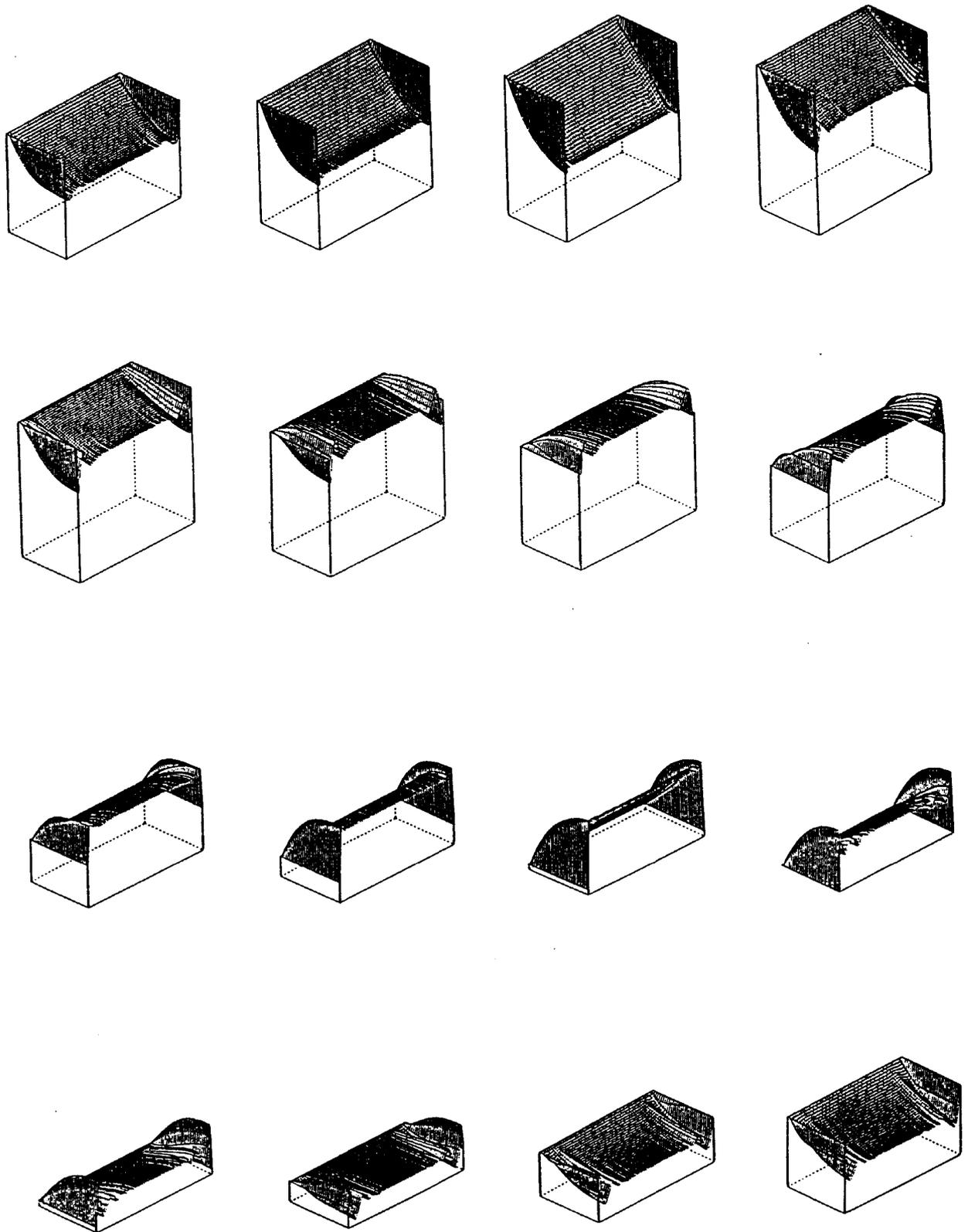
MAGNETIC FIELD
(MOST PART OF THE SLAB HAS CROSSED THE CURIE TEMPERATURE)

FIGURE 8
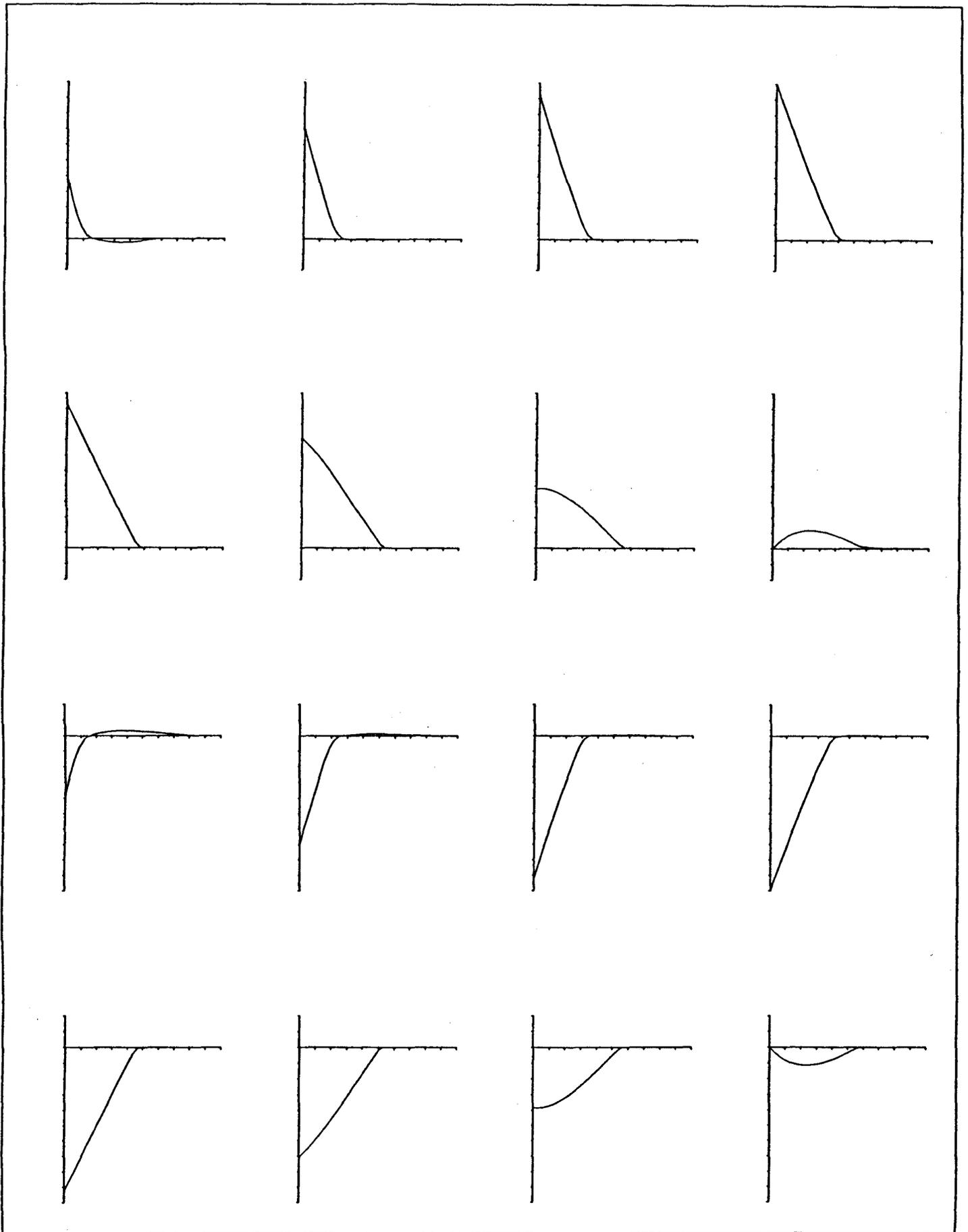
MAGNETIC FIELD FOR FIXED Y = b
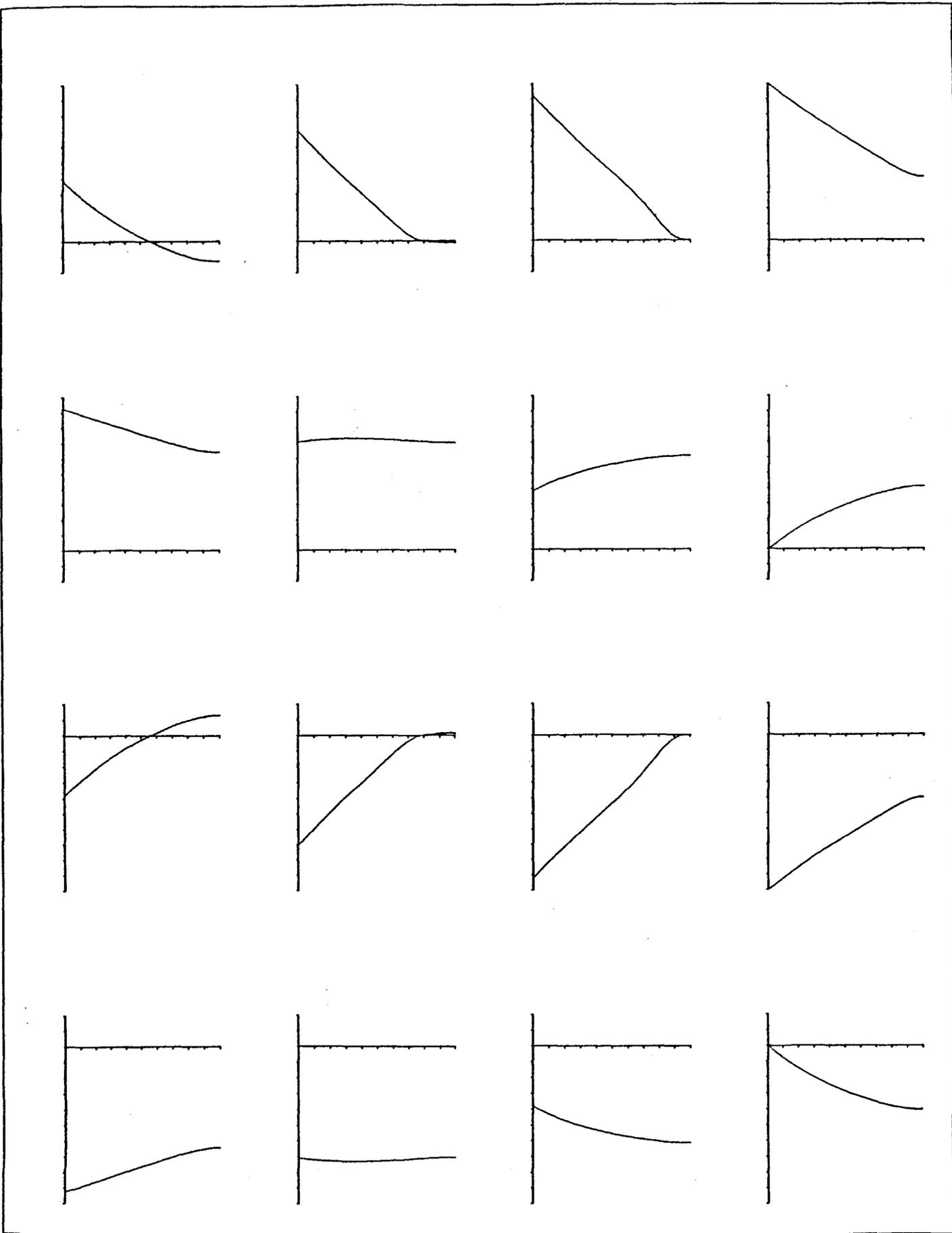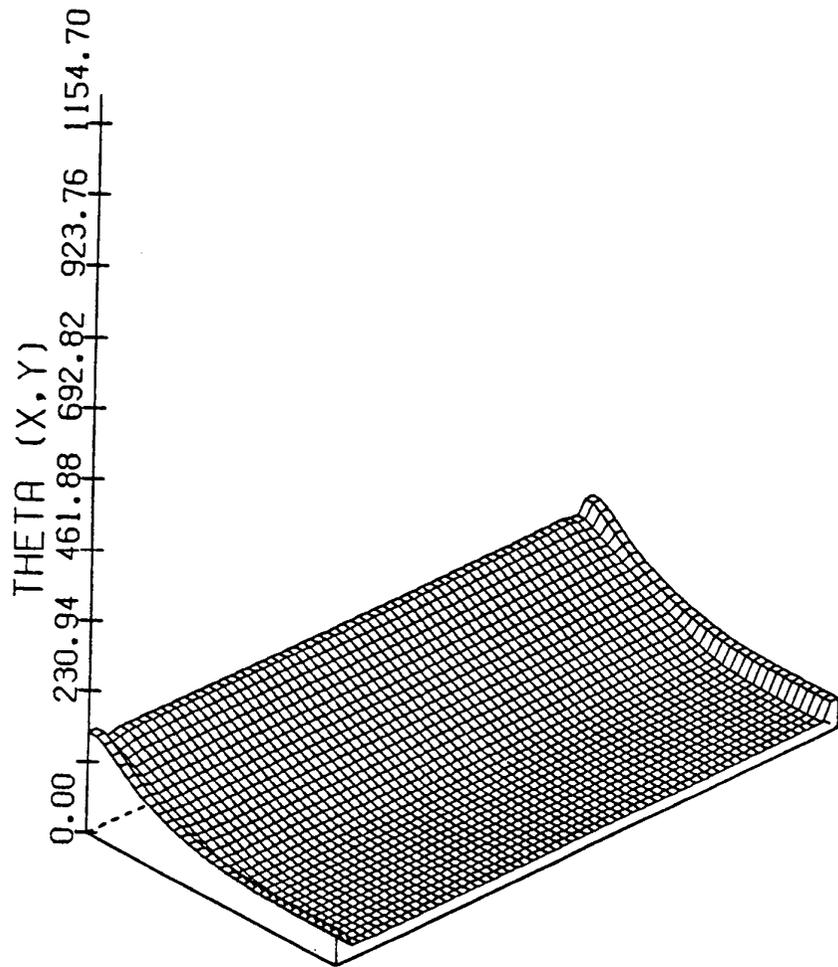**(AT THE BEGINNING OF THE HEATING)**

FIGURE 9

26
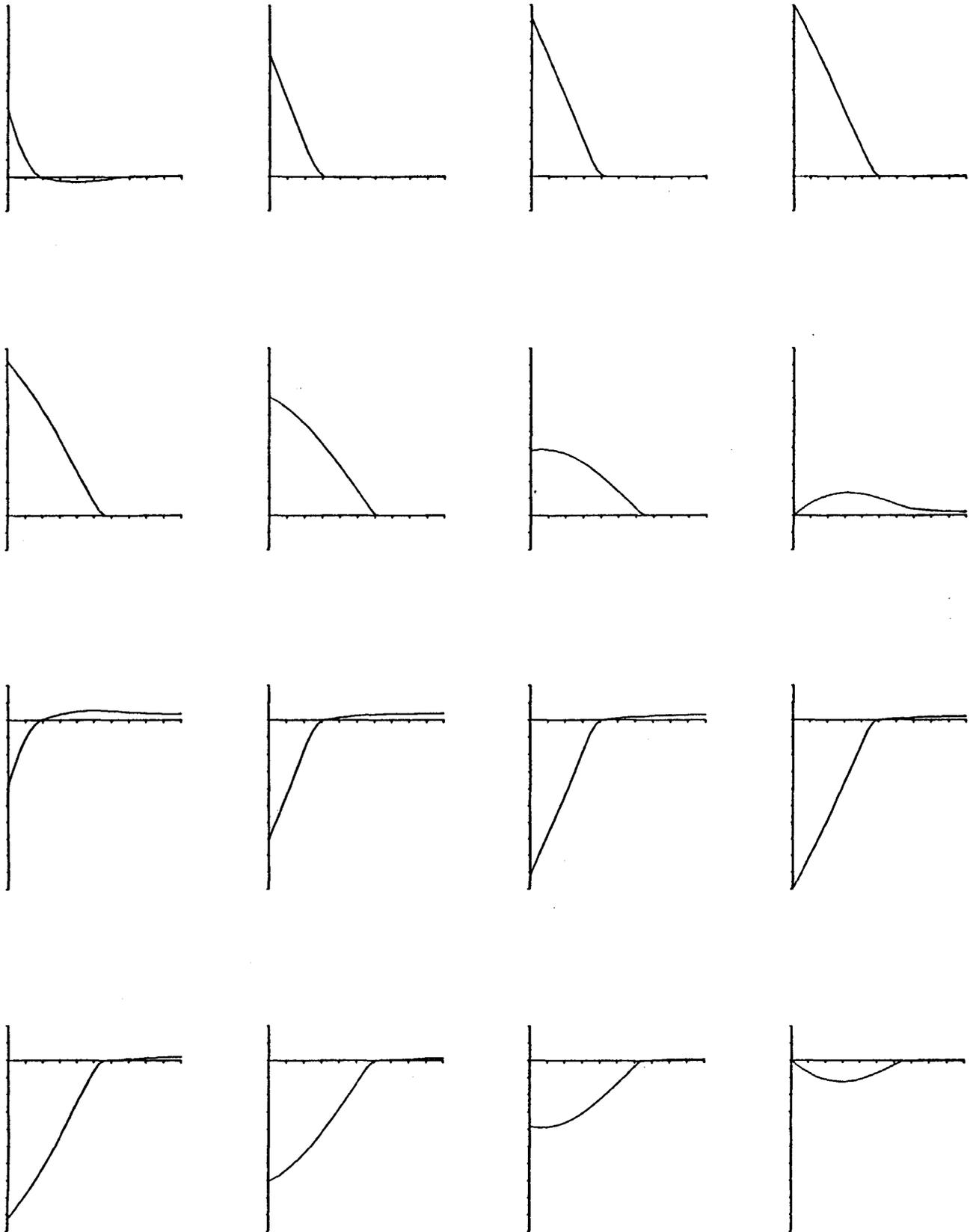
MAGNETIC FIELD FOR FIXED Y = b
(AFTER SOME HEATING)

FIGURE 10
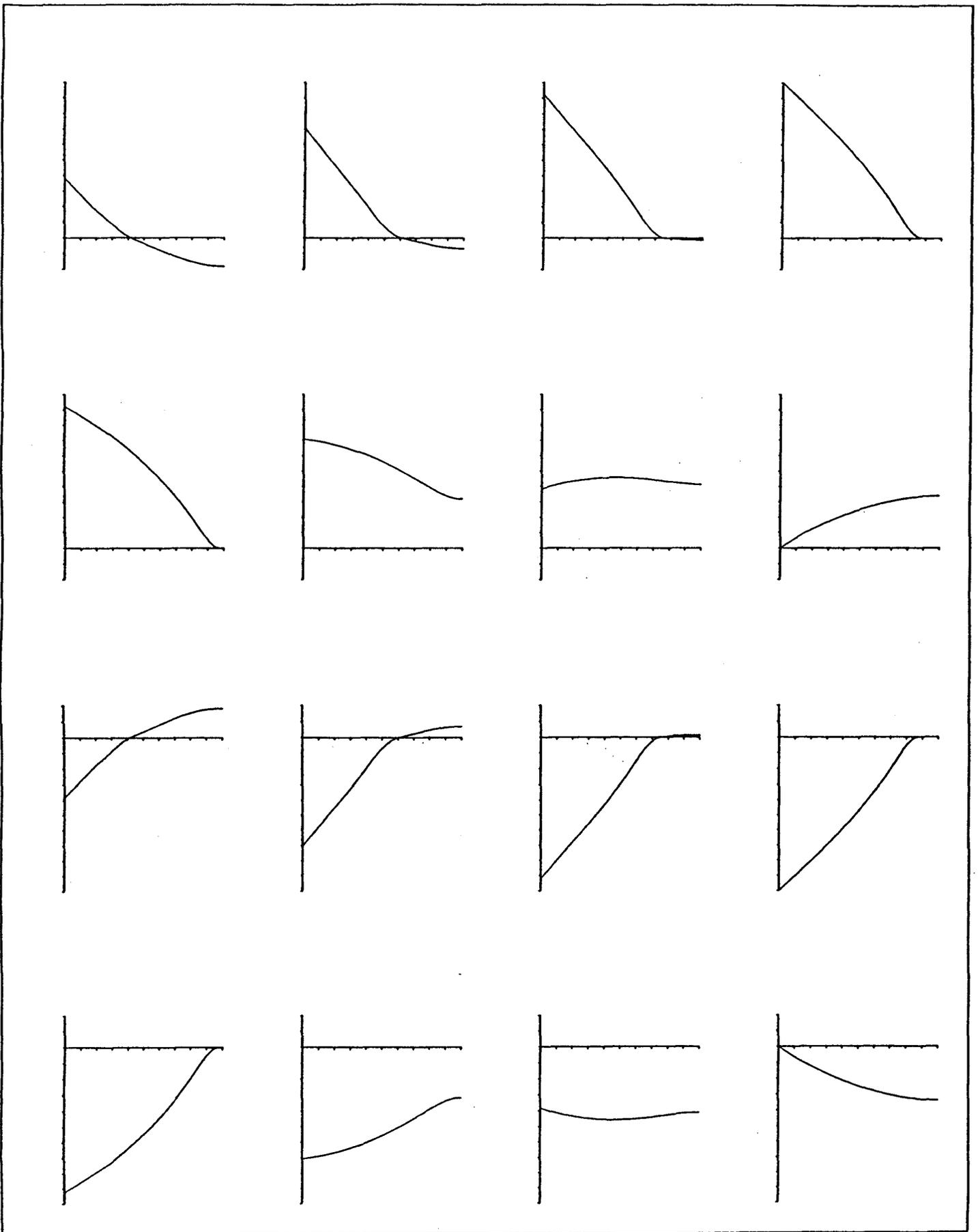
MAGNETIC FIELD FOR FIXED Y = b
(SURFACE HAS CROSSED THE CURIE TEMPERATURE)

FIGURE 11

28

MAGNETIC FIELD FOR FIXED Y = b
(MOST PART OF THE SLAB HAS CROSSED THE CURIE TEMPERATURE)

FIGURE 12

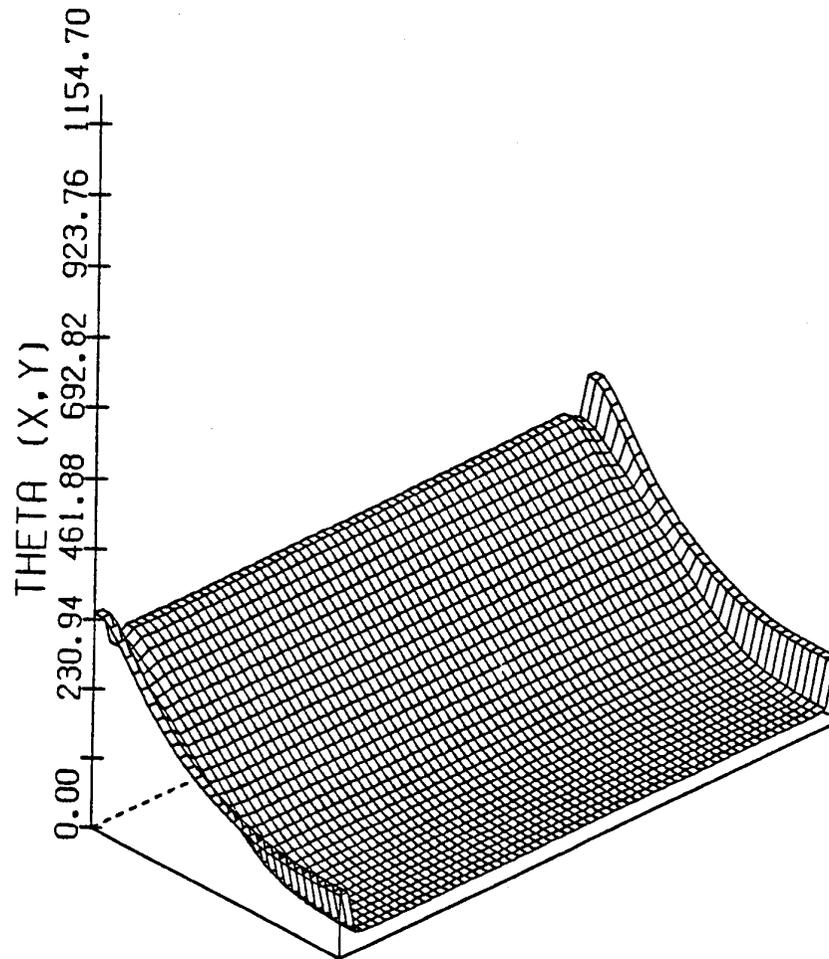FIGURE 13: TEMPERATURE DISTRIBUTION
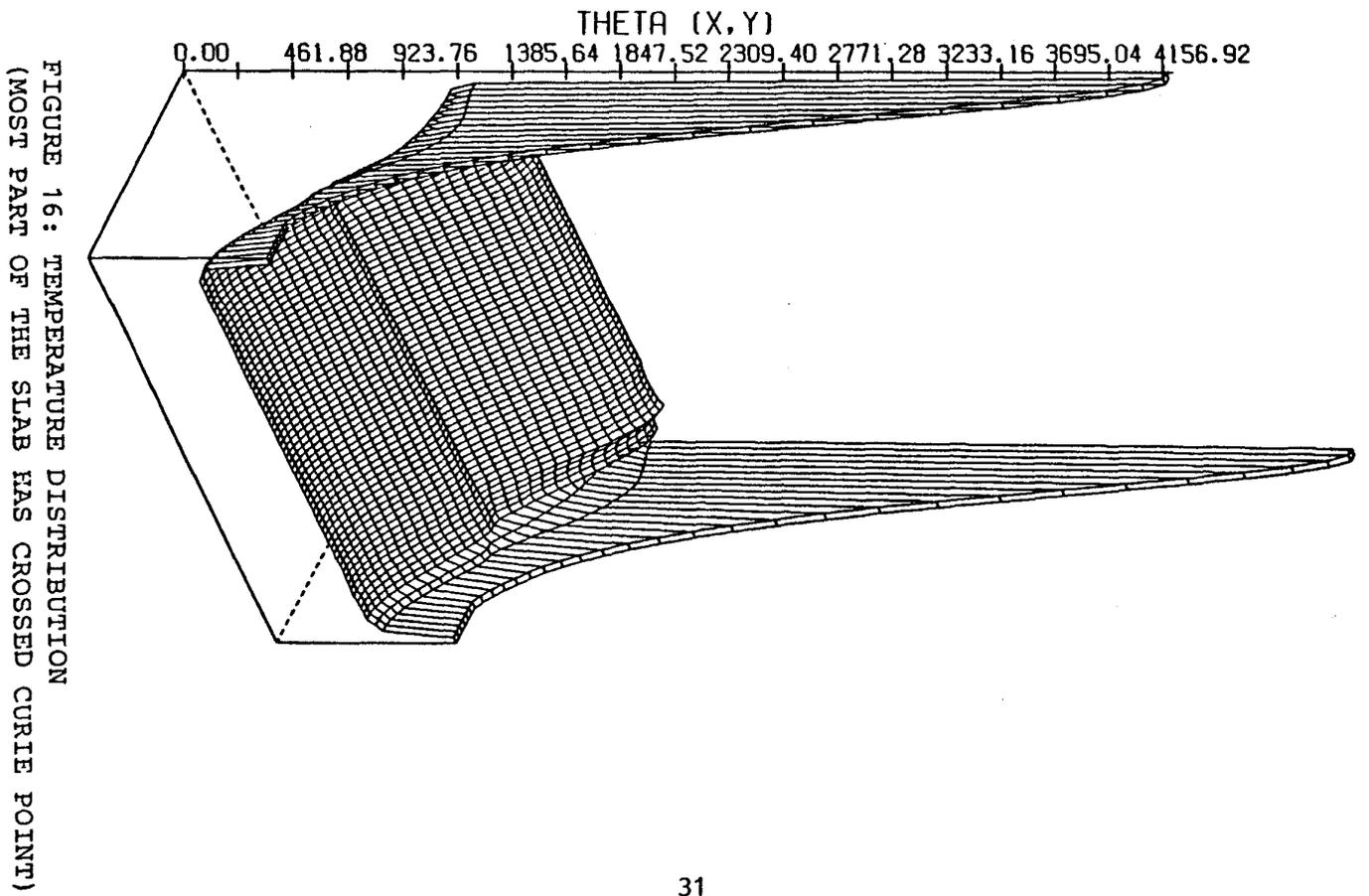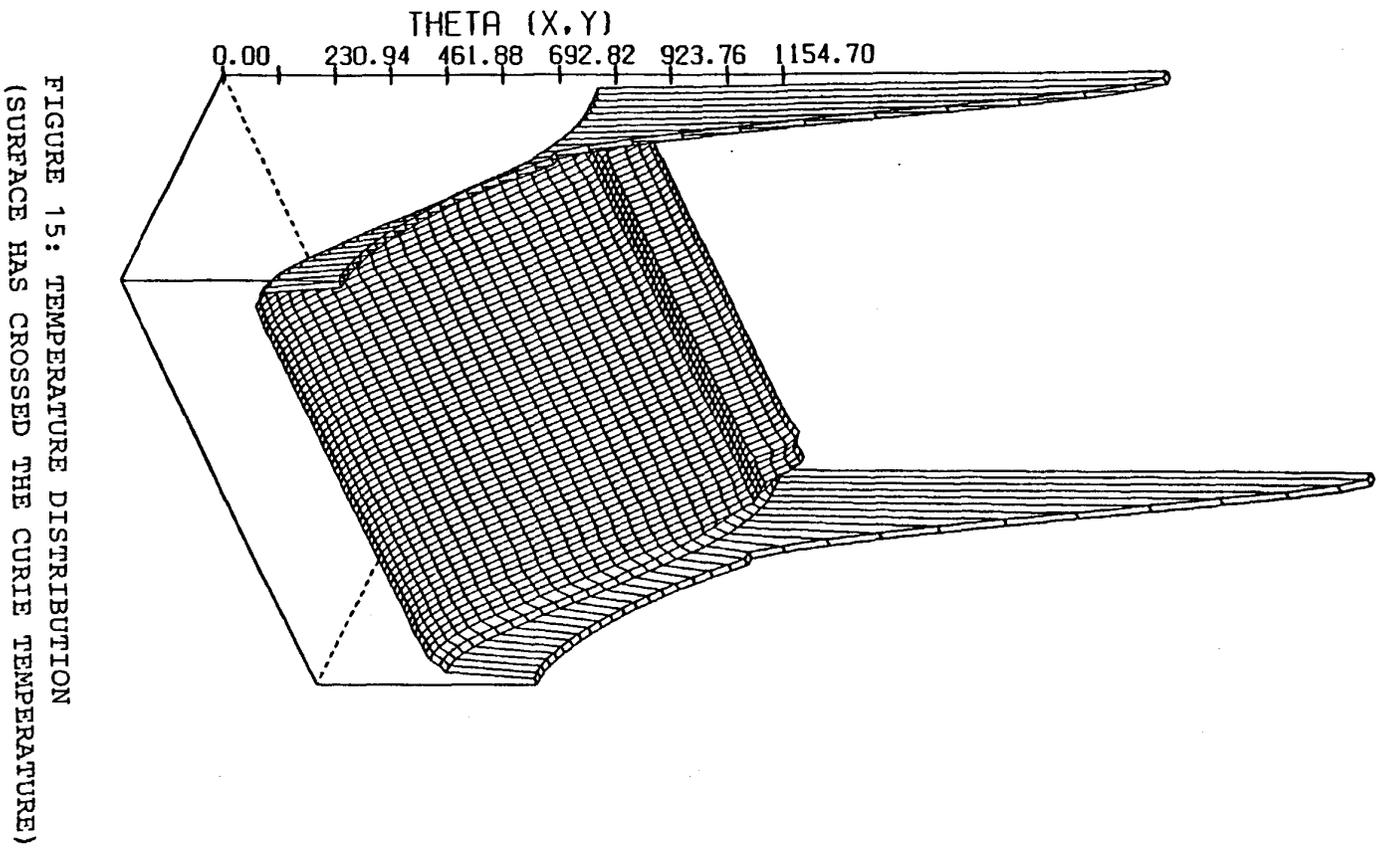(AT THE BEGINNING OF THE HEATING)

FIGURE 14: TEMPERATURE DISTRIBUTION
(AFTER SOME HEATING)

THETA (X,Y)

FIGURE 15: TEMPERATURE DISTRIBUTION
(SURFACE HAS CROSSED THE CURIE TEMPERATURE)

THETA (X,Y)

FIGURE 16: TEMPERATURE DISTRIBUTION
(MOST PART OF THE SLAB HAS CROSSED CURIE POINT)

31

5. Concluding Remarks

We have developed multi-grid algorithms for the numerical solution of a coupled system of two Stefan type equations representing a two-dimensional model of induction heating of large steel slabs. These algorithms allow the efficient numerical simulation of the induction heating process in much more reasonable CPU-times than by conventional single-grid techniques. What we did not consider in this paper was the optimal control of the heating procedure using e.g. the physical data H and/or ω as control parameters in order to achieve an almost uniform temperature distribution in minimal time which is much wanted in practice. The presented multi-grid algorithms may serve as an important tool in the numerical solution of such a constrained time-optimal control problem, a subject which will be investigated in subsequent work.